Available online at www.sciencedirect.com
ScienceDirect
Computational Materials Science xxx (2008) xxx–xxx
COMPUTATIONAL MATERIALS SCIENCE
www.elsevier.com/locate/commatsci

Modelling the carbon Snoek peak in ferrite: Coupling molecular dynamics and kinetic Monte-Carlo simulations

Sébastien Garruchet, Michel Perez *

MATEIS (ex-GEMPPM) – UMR CNRS 5510, Université de Lyon, INSA-Lyon, F69621, France

Received 31 May 2007; received in revised form 18 July 2007; accepted 8 November 2007

Abstract

Molecular statics, molecular dynamics and kinetic Monte-Carlo are used to model the carbon Snoek peak in ferrite. Using an interatomic EAM potential for the Fe–C system, saddle point energies for the diffusion of carbon have been evaluated under uniaxial stress by molecular statics. These energies have been reintroduced in a kinetic Monte-Carlo scheme to predict the repartition of carbon atoms in different octahedral sites. This repartition leads to an anelastic deformation calculated by molecular dynamics, which causes internal friction (the Snoek peak) for cyclic stress. This approach leads to quantitative predictions of the internal friction, which are in good agreement with experiments.

PACS: 62.40.+i; 61.43.Bn

Keywords: Internal friction; Fe–C alloys; Molecular dynamics; Kinetic Monte-Carlo; Snoek peak; Iron alloys

1. Introduction

In body-centred cubic (bcc) metals, like α-Fe, interstitial solute atoms are found in octahedral sites, which have the characteristic to be strongly non-symmetrical, leading to local strain distortions (cubic to tetragonal symmetry). These distortions can produce anelastic relaxation observable by dynamical mechanical measurements. Snoek [1] first discovered this relaxation by measuring the internal friction of an Fe–C sample as a function of temperature. He found that the relaxation amplitude was proportional to the carbon concentration.

This proportionality has been proved for a great amount of interstitial atoms (see the insightful review of Weller [2]) and therefore is very useful to quantify precisely the amount of interstitial atoms. The position of the peak is another important information that can be deduced from internal friction analysis. It is related to interactions between interstitial atoms and the iron matrix. As these interactions contain an elastic and a chemical part, their prediction, or modelling, is far from trivial.

The linear point defect theory [2,3] has been extensively used to describe the Snoek relaxation. However, non-linear effects, such as interaction of C with interstitial solute atoms or dislocations cannot be treated properly with this theory. Some previous studies tackled this problem either analytically [4] with fitting parameters or numerically [5] with empirical pairwise interatomic potentials.

In this paper, a general scheme at the atomic scale, able to account for non-linear effects, will be presented and validated on a simple Fe–C system. A molecular statics (MS) framework based on a recently published Fe–C embedded atom method (EAM) potential [6] is used to evaluate saddle point energies as a function of external applied stress. These saddle point energies serve as entry parameters of a kinetic Monte-Carlo (KMC) simulation that describes the kinetics of carbon jumps in interstitial sites. Then molecular dynamics (MD) is used to get the anelastic

* Corresponding author. Tel.: +33 4 72 43 80 63; fax: +33 4 72 43 85 39.
E-mail address: Michel.Perez@insa-lyon.fr (M. Perez).

0927-0256/$ - see front matter © 2007 Elsevier B.V. All rights reserved.
doi:10.1016/j.commatsci.2007.11.004

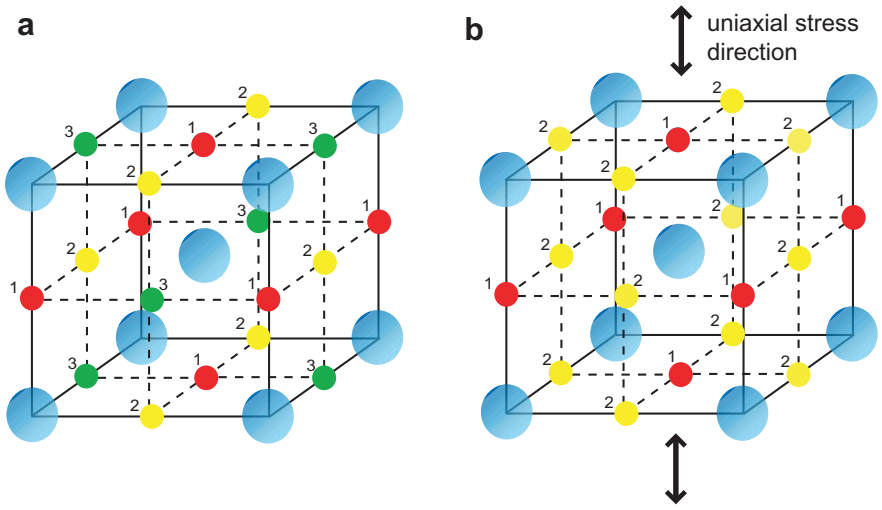

Fig. 1. (a) Three energetically equivalent octahedral sites in a stress free ferritic matrix. (b) Applying uniaxial stress leads to the formation of two energetically different octahedral sites: sites 1 (respectively 2) have their tetragonal distortion axis parallel (respectively perpendicular) to uniaxial stress direction.

distortion from the carbon population distribution (that comes out of KMC). Finally, form the applied stress and the resulting global strain, internal friction is calculated.

Some alternative approaches combined KMC with MD (*e.g.* radiation damages). In most of these works, MD results served as entry parameters for KMC [7,8]. Recent studies have tried to improve the coupling between the two methods, either by performing an "on the fly" combination of KMC and MD [9], or by extracting constitutive laws from MD calculations and incorporating them in KMC [10]. Our original scheme could be considered as a mixture of the two above mentioned techniques.

2. Snoek relaxation

Mechanical spectroscopy is a powerful experimental tool for characterising the Snoek relaxation. A cyclic stress $\sigma = \sigma_0 \cos(\omega t)$ is applied to a sample and the deformation $\epsilon = \epsilon_0 \cos(\omega t + \phi)$ is measured. The deformation can be decomposed as follows:

$$\epsilon = \epsilon_0' \cos(\omega t) + \epsilon_0'' \sin(\omega t) \tag{1}$$

with $\epsilon_0' = \epsilon_0 \cos(\phi)$ being the strain component in phase with stress (elastic deformation: $\sigma = \epsilon' E, E$: Young's modulus) and $\epsilon_0'' = \epsilon_0 \sin(\phi)$ the stain component in quadrature with stress.

The internal friction δ is defined as the ratio of the dissipated energy during one cycle (ΔW) over the maximum elastic energy (W_{el})

$$\delta = \frac{\Delta W}{W_{\text{el}}} = \frac{\int_0^{\frac{2\pi}{\omega}} \sigma \, \mathrm{d}\epsilon''}{\frac{1}{2}\sigma_0 \epsilon_0'} = 2\pi \frac{\epsilon_0''}{\epsilon_0'} = 2\pi \tan\phi \tag{2}$$

Internal friction is often referred to as $Q^{-1} = \delta/(2\pi) = \tan\phi$.

In the case of carbon in bcc iron, there are three types of octahedral sites (1, 2 and 3), which are energetically equivalent in a stress free state (Fig. 1a). Application of a uniaxial stress σ, splits the energy levels such that one site, called "site 1"[1], is different from the two others, called "site 2"[2] in the following (see Fig. 1b).

At low applied stresses (linear point defect theory), carbon jump frequency ν does not depend on stress or site types and follows an Arrhenius equation: $\nu = \nu_0 \exp[-\Delta G_0/(kT)]$, where ΔG_0 is the diffusion barrier of carbon and ν_0 the jump attempt frequency. Within the linear point defect theory [2], the system undergoes a relaxation with inverse time $\tau^{-1} = 3\nu$. Internal friction is then given by a Debye equation

$$Q^{-1} = \frac{\Delta\omega\tau}{1 + (\omega\tau)^2} \tag{3}$$

where Δ is the relaxation strength and $Q^{-1}_{\text{Max}} = \Delta/2$ is the internal friction maximum value.

To avoid the former assumption of linearity and propose a more general framework for modelling the Snoek relaxation, we need to evaluate: (i) the stress dependence of saddle point energies; (ii) the carbon distribution in each site type versus time; (iii) the anelastic deformation for a given carbon distribution. Each of these steps will be detailed in the following section.

3. Modelling internal friction: the method

3.1. Saddle point energies versus stress

To analyse the evolution of the diffusion barrier with external stress, a conjugate gradient procedure has been applied to a system of 2000 iron atoms and 1 carbon atom.

[1] With tetragonal distortion axis parallel to uniaxial stress direction.

[2] Formerly sites 2 and 3 of Fig. 1a, with tetragonal distortion axis perpendicular to uniaxial stress direction.

Please cite this article in press as: S. Garruchet, M. Perez, Comput. Mater. Sci. (2008), doi:10.1016/j.commatsci.2007.11.004

To apply an uniaxial stress state to the system, the box dimension in the traction axis has been adjusted, leaving the two other dimensions stress free. The energy barrier for C atom migration was estimated by displacing the C atom and allowing it to relax in the plane perpendicular to the jump direction, whilst the Fe atoms relaxed fully.

Fig. 2 shows the variation of the diffusion barrier when a carbon atom jumps from an octahedral site of type 1 to an octahedral site of type 2 (or 3): ΔG_{12} (and respectively from an octahedral site of type 2 (or 3) to an octahedral site of type 1: ΔG_{21}) as a function of the applied stress. As expected, there is an energetically favoured site depending on the applied stress (traction or compression): site 1 is favoured under traction and site 2 (or 3) is favoured under compression. Indeed, the two first neighbours of site 1 are moved aside under traction, leaving more space for the carbon atom.

From these results, two equations can be fitted

$$\begin{cases} \Delta G_{12} = -\beta\frac{\sigma^2}{2} + \alpha\sigma + \Delta G_0 \\ \Delta G_{21} = -\beta\frac{\sigma^2}{2} - \alpha\sigma + \Delta G_0 \end{cases} \quad (4)$$

where $\alpha = (24.4 \pm 0.5) \times 10^{-3}$ eV/GPa and $\beta = (12 \pm 1) \times 10^{-3}$ eV/GPa^2. $\Delta G_0 = 0.849 \pm 0.002$ eV is the diffusion barrier of a carbon in a stress free ferrite matrix for the present iron–carbon potential [6]. This non-linearity is not surprising considering (i) the non-symmetrical geometry of octahedral sites; (ii) the anharmonicity of the Fe–C potential.

The justification of this simple form could be understood as follows. The energy barriers from site i to site j is given by

$$\Delta G_{ij}(\sigma) = G_{sp}(\sigma) - G_i(\sigma) \quad (5)$$

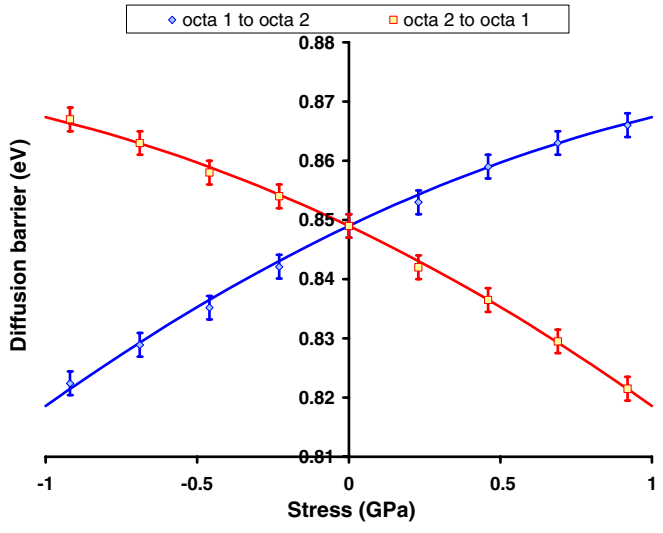

Fig. 2. Variation of the carbon diffusion barrier to jump from an octahedral site 1 to an octahedral site 2 (or 3), respectively from an octahedral site 2 (or 3) to octahedral site 1 as function of the applied stress to the system during a uniaxial stress test.

The saddle point energy, G_{sp}, which corresponds to the tetragonal site energy, is relatively insensitive to uniaxial traction (no volume change of tetragonal site at first order), leading to

$$G_{sp}(\sigma) \approx G^0_{sp} \quad (6)$$

However, due to our Fe–C potential, energies of sites 1 and 2 depend non-linearly on the uniaxial stress state

$$G_1(\sigma) \approx G^0_1 + \left.\frac{\partial G_1}{\partial\sigma}\right|_{\sigma=0}\sigma + \left.\frac{\partial^2 G_1}{\partial\sigma^2}\right|_{\sigma=0}\frac{\sigma^2}{2} \quad (7)$$

$$G_2(\sigma) \approx G^0_2 + \left.\frac{\partial G_2}{\partial\sigma}\right|_{\sigma=0}\sigma + \left.\frac{\partial^2 G_2}{\partial\sigma^2}\right|_{\sigma=0}\frac{\sigma^2}{2} \quad (8)$$

Due to the symmetry of our system, uniaxial traction has the same effect on site 1 energy as uniaxial compression on site 2 energy, leading to

$$\alpha = \left.\frac{\partial G_2}{\partial\sigma}\right|_{\sigma=0} = -\left.\frac{\partial G_1}{\partial\sigma}\right|_{\sigma=0} \quad (9)$$

$$\beta = \left.\frac{\partial^2 G_1}{\partial\sigma^2}\right|_{\sigma=0} = \left.\frac{\partial^2 G_2}{\partial\sigma^2}\right|_{\sigma=0} \quad (10)$$

with $\alpha > 0$ (geometric effect) and $\beta > 0$ (non-linearity of the Fe–C potential) justifying then both the form of Eq. (4) and the sign of α and β coefficients.

3.2. Kinetics of defects distribution and anelastic deformation

KMC is used to evaluate the kinetics of defects distribution. KMC is based on the evaluation of the probabilities of any possible event that can occur at a given time [11]. The sum of these probabilities is related to the residence time τ_R of a given state of the system.

Let us start with a system with a given configuration i and an associated energy E_i. This system has Z possible transitions from this configuration i to a neighbouring configuration j. Each transition j involve the crossing of a saddle point (intermediate state of higher energy E^j_{sp}). The energy barrier corresponding to the jth transition is $\Delta G_{ij} = E^j_{sp} - E_i$ with associated probability

$$p_{i\to j} = \exp\left(\frac{\Delta G_{ij}}{kT}\right) \quad (11)$$

The probability that this transition occurs during time interval dt is then

$$w_0 p_{i\to j}\,dt = w_0 \exp\left(\frac{\Delta G_{ij}}{kT}\right)dt = w_k\,dt \quad (12)$$

where w_k is the probability per unit time that the kth transition occurs and w_0 is the attempt frequency.

The probability that no event occurs during time interval $\delta t = n\,dt$ is

$$\left(1 - \sum_k^Z w_k\,dt\right)^n \approx \exp(-\Omega\delta t) \quad (13)$$

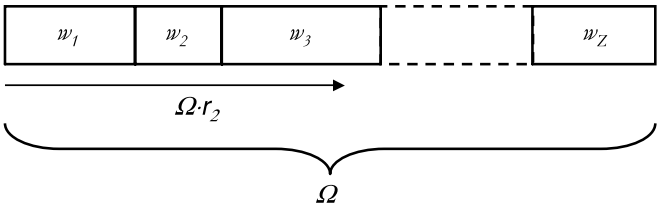

Fig. 3. The selected transition is the one that intercepts the end of the segment of length $\Omega \cdot r_2$. In this example, it would be the third one.

where $\Omega = \sum_k^Z w_k$. The residence time τ_R of the configuration i is then evaluated by picking a random number r_1 between 0 and 1 and applying

$$\tau_R = -\frac{\ln r_1}{\Omega} \tag{14}$$

To select the actual transition that will be performed after a time τ_R, a second random number r_2 between 0 and 1 is used. The selected transition is the one that intercepts the end of the segment of length $\Omega \cdot r_2$ (see Fig. 3).

In the case of carbon in iron, each carbon atom has four neighbouring octahedral sites. If n_C is the number of carbon atoms in the MD simulation box, the number of possible transition is $Z = 4n_C$. Each atom of type 1 can jump in four sites of type 2 and each atom of type 2 and can jump in two sites of type 1 and two sites of 2 (see Fig. 1b), leading to the transition probabilities

$$p_{1\to 2} = 4\exp\left(\frac{\Delta G_{12}}{kT}\right) \tag{15}$$

$$p_{2\to 1} = 2\exp\left(\frac{\Delta G_{21}}{kT}\right) \tag{16}$$

$$p_{2\to 2} = 2\exp\left(\frac{\Delta G_0}{kT}\right) \tag{17}$$

Note that the jump attempt frequency v_0 of linear point defect theory (see Section 2) is twice the attempt frequency w_0 used in KMC. This is due to the existence of two transition paths from site i to site j (see Fig. 1b).

At each KMC step: (i) *stress* is calculated for time t: $\sigma = \sigma_0 \cos(\omega t)$; (ii) *energy barriers* $\Delta G_{ij}(\sigma)$ given in the preceding section (Eq. (4)) are updated; (iii) one of the $4n_C$ possible transitions is chosen, giving a new *carbon distribution* (C_1 and C_2) in sites 1 or 2; (iv) *residence time* τ_R is calculated and time is updated ($t \leftarrow t + \tau_R$); (v) *anelastic deformation* ϵ^{an} is evaluated from MD simulations on preceding carbon distribution (C_1 and C_2). The five preceding steps are repeated until a stationary state is reached (usually after a few periods)[3]. Finally, *internal friction* is calculated using Eq. (2).

MD simulations, performed on stage (v) when C_1 and C_2 oscillations reach a stationary state, have been run with LAMPPS [12] keeping number of atoms, pressure and temperature constant (NPT) within periodic boundary conditions. MD simulations have been performed with a few tenths of carbon atoms, on different simulation box sizes, inversely proportional to the carbon concentration, until the system reaches an equilibrium (around 200 000 time-steps). The MD simulation box deformation along direction 1 (ϵ_{11}) has then been averaged during the following 200 000 time-steps, giving thus the anelastic deformation. Note that MD simulation time (a few hundreds of ps) is not taken into account because it is negligible compared to KMC carbon diffusion time ($\approx$1s) in the range of temperature concerned by this study.

4. Results

In this section, calculated internal friction will be presented as a function of temperature, frequency and carbon content. It will be compared with experimental data. In the following, the value of the attempt frequency will be chosen to remain in the range of those found in the literature ($v_0 = 9 \times 10^{13}$ Hz) and $\sigma_0 = 0.131$ GPa($\epsilon_0 = 0.1\%$) will be used to be as consistent as possible with experimental conditions. In the last part, we point out the effect of the diffusion barrier non-linearity on the Snoek peak.

4.1. Temperature and frequency

Fig. 4 represents the variation of internal friction[4] versus temperature for frequencies of 0.5, 1 and 2 Hz. As expected, internal friction exhibits a peak at room temperature (*i.e.* the so called Snoek peak). Moreover, it can be noticed that low frequencies shift the peak to lower temperatures (respectively high frequencies shift the peak to higher temperatures), as observed experimentally. However, frequency has no influence on internal friction maximum value. This can be easily established, if we superimpose the three curves on each other by a horizontal shift on the temperature scale, as shown in the inset of the Fig. 4. In the following, the frequency of 1 Hz was used as in many internal friction experiments on Fe–C system. In Fig. 4, simulated internal friction is compared with linear point defect theory (Eq. (3) with Δ fitted[5]): both approaches fit remarkably well, thus validating the coupled MD/KMC approach.

4.2. Carbon content

Fig. 5 shows the Snoek peak for the five different carbon concentrations (0.01%, 0.05%, 0.1%, 0.5% and 1% atomic).

[3] Stage (v) is not necessarily performed at each KMC step. Indeed ϵ^{an} should be computed rather often to accurately describe anelastic deformation oscillations. However if performed at each KMC step ϵ^{an} calculation would lead to intractable computing times.

[4] Uncertainties inerrant to our approach have been estimated to be $\Delta Q^{-1} = 1.5$ [C(% at.)]. For the sake of clarity, corresponding error bars were reported only on Fig. 4.

[5] Comparison between experimental and modelled peak amplitude is detailed in Section 4.3.1.

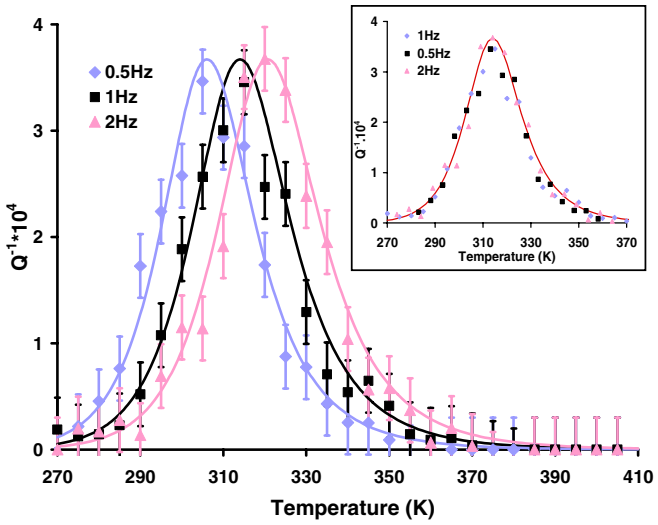

Fig. 4. Modelled Snoek peak for different frequency. Coupled MD/KMC simulated internal friction (points) is compared with linear point defect theory (lines-Eq. (3)): both approach fit remarkably well. The inset shows the three curves superimposed on each other after an horizontal shift of temperature.

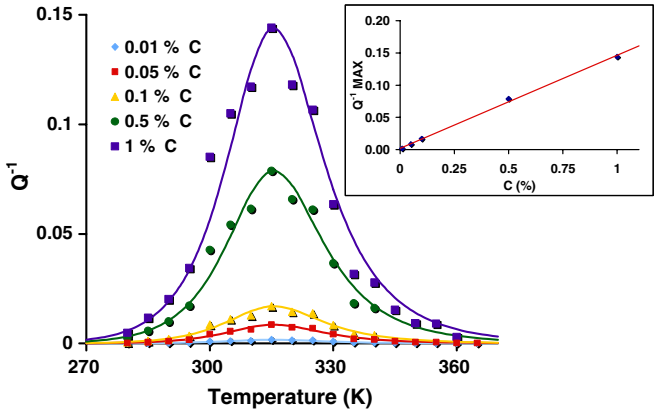

Fig. 5. Modelled Snoek peak in Fe–C for different carbon concentration. The inset show the evolution of the carbon concentration versus internal friction maximum value Q^{-1}_{Max}: internal friction depends linearly on carbon content.

The internal friction peak is localised at a temperature of 314 K for all carbon concentrations.

It can be noticed that internal friction values seem to be proportional to the carbon content, as observed experimentally. Indeed, the internal friction maximum Q^{-1}_{Max} is assumed to be directly proportional to the carbon content in solid solution [13], and follows the relation:

$$Q^{-1}_{\mathrm{Max}} = K \cdot [\mathrm{C}(\%\mathrm{at.})] \tag{18}$$

where K is a constant. The inset on Fig. 5 depicts the dependence of the maximum value of the internal friction with the carbon concentration. As experimentally, the internal friction maximum Q^{-1}_{Max} is proportional to the carbon content with a value of the constant $K = 0.15$ (% at.)$^{-1}$.

4.3. Experimental versus simulated Snoek peak

Internal friction experiments are generally performed on polycrystalline samples (torsion test), whereas our approach considers a tensile test on a monocrystalline sample (traction axis [100]). A relationship between $\Delta_{E_{100}}$ (relaxation strength for traction on monocrystal) and Δ_G (relaxation strength for torsion on polycrystal) is then needed.

4.3.1. From simulation (traction on monocrystal) to experiment (torsion on polycrystal)

In the frame of linear point defect theory, relaxation strength is given, depending on solicitation type [2]

$$\Delta_E = \frac{2}{9}\frac{C_0 v_0}{k_B T}(\lambda_1 - \lambda_2)^2 E(\Gamma)(1 - 3\Gamma) \tag{19}$$

$$\Delta_G = \frac{4}{3}\frac{C_0 v_0}{k_B T}(\lambda_1 - \lambda_2)^2 G(\Gamma)\Gamma \tag{20}$$

where C_0 is the concentration of carbon, v_0 the atomic volume, $(\lambda_1 - \lambda_2)$ the carbon induced tetragonal distortion, G the shear modulus, E the Young modulus and Γ the orientation parameter describing the misorientation between mechanical solicitation and basis axis of the cubic lattice.

In our work, the orientation parameter $\Gamma = 0$ because the traction axis is parallel to the [100] direction. Young's modulus in the [100] direction corresponding to our potential is $E_{100} = 131$ GPa, in agreement with experimental data [14]. For a polycrystal, the mean value of the orientation parameter is considered to be $\langle\Gamma\rangle = 0.2$ [15].

Correspondence between relaxations strength $\Delta_{E_{100}}$ (traction on monocrystal) and Δ_G (torsion on polycrystal) is then given by the ratio of Eqs. (19) and (20)

$$\frac{\Delta_G}{\Delta_{E_{100}}} = \frac{6G\langle\Gamma\rangle}{E_{100}} \approx 0.74 \tag{21}$$

To be compared to experimental values resulting from torsion on polycrystals, our results should then be multiplied by 0.74.

4.3.2. Results

Coupled MD/KMC simulation of a ferrite matrix with 20 at. ppm (particles per million) carbon in solid solution was performed to compare to Weller's experimental results [15].

It can be observed in Fig. 6 that both experiment and modelling have the peak position at the same temperature: 314 K. After subtraction of the experimental background (defects of the ferrite matrix, grain boundary, ...), the agreement is quite satisfactory in terms of shape and peak amplitude.

Moreover, the same agreement is observed for the constant K linking the carbon concentration to the internal friction maximum value Q^{-1}_{Max}. Our modified value $K = 0.15 \times 0.74 = 0.11$ is relatively close to the experimental value of Saitoh et al. [16] $K = 0.14$ (% at.)$^{-1}$.

Please cite this article in press as: S. Garruchet, M. Perez, Comput. Mater. Sci. (2008), doi:10.1016/j.commatsci.2007.11.004

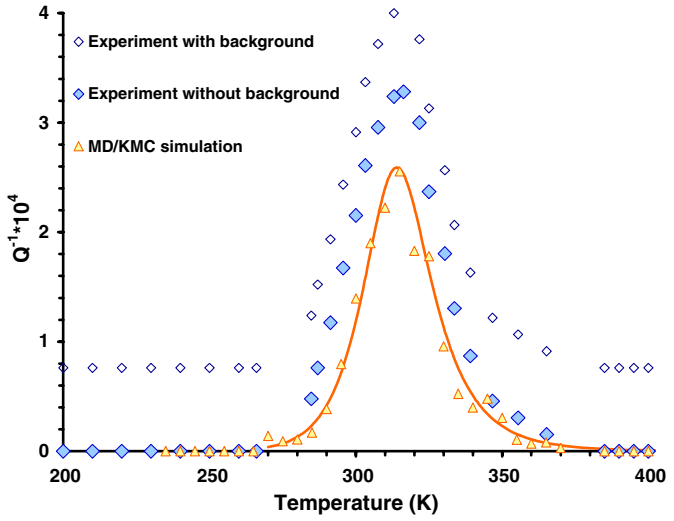

Fig. 6. Comparison between simulated and experimental (from [15]) Snoek peaks in Fe–C system with 20 at. ppm. Without any adjustable parameter, coupling KMC with MD gives a good description of the Snoek peak.

It is clear that our results underestimate internal friction by $\approx 25\%$. Nevertheless, this difference is not due to our coupled MD/KMC approach, but is certainly the consequence of our Fe–C potential, which underestimates the local elastic distortion $(\lambda_1 - \lambda_2)$. Indeed in a previous paper [6], we showed that this potential underestimates the expansion of the carbon induced tetragonal lattice distortion.

4.4. Non-linearity of diffusion barrier

To underline the influence of non-linearity on the Snoek peak shape, a coupled MD/KMC simulation with a high value of σ_0 (2.6 GPa, $\epsilon_0 \approx 2\%$) using non-linear stress dependence on diffusion barrier from Eq. (4), has been compared with linear point defect theory (Eq. (3)).

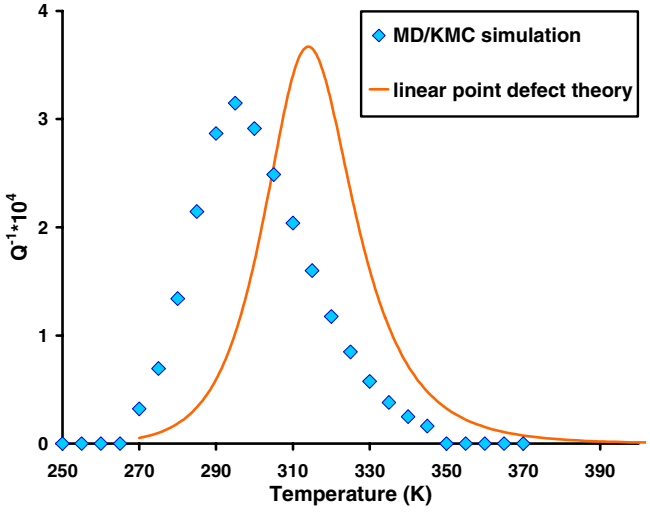

Fig. 7. Modelled Snoek peak with non-linear stress dependence on diffusion barrier (diamonds) for a value of $\sigma_0 = 2.6$ GPa ($\epsilon_0 \approx 2\%$) and linear point defect theory from Eq. (3) (line).

It could be noticed on Fig. 7 that the non-linearity of the diffusion barrier have a strong influence on the peak shape and amplitude for large stresses. Moreover, in the prospective case of carbon ↔ substitutional atom interactions, or carbon ↔ dislocation interactions (purpose of a forthcoming paper), where local stresses (or stains) are important, the influence of non-linearity is far from being negligible. The use of our coupled MD/KMC approach, validated in the linear case, is then fully justified.

5. Conclusion

This work proves that coupling molecular statics, molecular dynamics and kinetic Monte-Carlo is a useful method to model the Snoek peak. MS was used to predict the stress dependence of energy barriers. KMC was used to predict the evolution of carbon distribution in sites 1 or 2 for a cyclic applied stress. Then, MD was performed to evaluate the anelastic deformation for a given carbon distribution in sites 1 or 2.

Results obtained in terms of Snoek peak: (i) shape; (ii) position versus temperature and frequency; (iii) amplitude versus carbon content, are in good agreement with various data taken from the literature.

Once successfully compared with existing models and experiments in the linear domain, this technique could be straightforwardly applied to non-linear problems, such as interactions between substitutional elements (Mn, Cr, V,...) or dislocations and interstitial atoms (C, N). These interactions are indeed at the base of: (i) interstitial free (IF) steels specific properties; (ii) the understanding of precipitation first stages in steels. Although such interactions are well documented experimentally [16,13,17,18], they are not clearly understood. Coupling MD and KMC will be all the more powerful as a large effort is currently made to develop new interatomic potentials for metals and alloys [19–23].

References

[1] J.L. Snoek, Physica 8 (7) (1941) 711–733.
[2] M. Weller, in: Mechanical spectroscopy Q^{-1}, Trans. Tech. Pub., 2001, p. 683.
[3] P. Debye, Polar Molecules, Chemical Catalog Co, New York, 1929, p. 172.
[4] Y. Wang, M. Gu, L. Sun, K.L. Ngai, Phys. Rev. B 50 (6) (1994) 3525–3531.
[5] H. Numakura, G. Yotsui, M. Koiwa, Acta Metall. Mater. 43 (2) (1995) 705–714.
[6] C.S. Becquart, J.M. Raulot, G. Benecteux, C. Domain, M. Perez, S. Garruchet, H. Nguyen, Comput. Mater. Sci. 40 (2007) 119–129.
[7] Q. Xu, H.L. Heinich, T. Yoshiie, J. Comp-Aided Mater. Des. 6 (1999) 215–223.
[8] M.J. Caturla, N. Soneda, E. Alonso, B.D. Wirth, T.D. Delarubia, J.M. Perlado, J. Nucl. Mater. 276 (2000) 13–21.
[9] G. Betz, W. Husinsky, Nucl. Instrum. Meth. B 193 (2002) 352–358.
[10] D. Kulikov, L. Malerba, M. Hou, Nucl. Instrum. Meth. B 228 (2005) 245–249.

[11] T.A. Abinandanan, F. Haider, G. Martin, Acta Mater. 46 (12) (1998) 4243–4255.
[12] LAMMPS, <http://lammps.sandia.gov/>.
[13] V. Massardier, E. Lepatezour, L. Soler, J. Merlin, Metall. Trans. A 36A (2005) 1745–1755.
[14] J. Adams, D.S. Agosta, R.G. Leisure, H. Ledbetter, J. Appl. Phys. 100 (2006) 113530.
[15] M. Weller, Mater. Sci. Eng. A 442 (1–2) (2006) 21–30.
[16] H. Saitoh, N. Yoshinaga, K. Ushioda, Acta Mater. 52 (2004) 1255–1261.
[17] Y. Saito, Mater. Sci. Eng. A A223 (1997) 134–145.
[18] H. Numakura, M. Koiwa, J. Phys. IV 6 (C8) (1996) 97–106.
[19] V. Sorkin, E. Polturak, J. Adler, Phys. Rev. B 68 (2003) 174102.
[20] G.J. Ackland, M.I. Mendelev, D.J. Srolovitz, S. Han, A.V. Barashev, J. Phys.: Condens. Mat. 16 (2004) S2629–s2642.
[21] C. Domain, C.S. Becquart, J. Foct, Phys. Rev. B 69 (2004) 144112.
[22] A. Caro, D.A. Crowson, M. Caro, Phys. Rev. Lett. 95 (2005) 075702.
[23] R.F. Zhang, Y. Kong, B.X. Liu, Phys. Rev. B 71 (2005) 214102.

Please cite this article in press as: S. Garruchet, M. Perez, Comput. Mater. Sci. (2008), doi:10.1016/j.commatsci.2007.11.004